

# Hofmeister Effect and Electrostatic Interaction Enhanced Ionic Conductive Organohydrogels for Electronic Applications

Yinghong Wu, Yijie Mu, Yang Luo,\* Carlo Menon, Zhiwen Zhou, Paul K. Chu, and Shien-Ping Feng\*

The emerging cryoprotectant replacement method endows hydrogels with nondrying and antifreezing properties, but the low conductivity still limits wider electronic applications. In this work, the Hofmeister effect and electrostatic interaction are introduced to improve the conductivity of organohydrogels and their enhancement mechanism are studied in depth. The Hofmeister effect mainly influences the physical properties, such as the pore structure and mechanical strength, which subsequently impacts ion transfer during the solvent replacement process. The lithium and sodium bonds formed by the electrostatic interaction play a more important role in the conductivity of organohydrogels and an overall picture is presented based on the synergistic enhancement of the Hofmeister effect and electrostatic interaction to achieve highly ionic conductive organohydrogels. The champion organohydrogels are applied as soft ionic conductors and antireflective layers in triboelectric, photovoltaic, and thermoelectric applications. The proposed mechanism advances the understanding of the contribution of ions to organohydrogels for wearable electronics.

have aroused increasing research interest due to the high transparency, stretchability, and biocompatibility.<sup>[8–10]</sup> However, hydrogels dry easily consequently negatively impacting the operation temperature window, service lifetime, as well as applications. The advent of the solvent replacement method, simply replacing water with cryoprotectant (CPA) in the hydrogels, has realized organohydrogels with better resistance against drying and freezing for long-term applications under extreme conditions.<sup>[11–15]</sup>

However, the major issue plaguing CPA replacement is the non-negligible conductivity decrease of organohydrogels during the solvent immersion process, which significantly limits its use as an ionic conductor in electronic applications. There have been several attempts to solve the problem.<sup>[16–19]</sup> One of the common techniques is to dissolve inorganic salts in the

## 1. Introduction

The growing popularity of flexible and wearable electronics has triggered large demand for soft conductors.<sup>[1–3]</sup> In recent years, soft ionic conductors have gained much attention in applications such as electronic skins, skin-like sensors, human-machine interfaces, and soft robots.<sup>[4–7]</sup> In particular, hydrogels


replacement solvent to generate ionic conductive organohydrogels. For example, Song et al.<sup>[16]</sup> immersed poly(ethylene glycol) diacrylate hydrogel fibers in a solution consisting of glycerin, water, and KCl/CaCl<sub>2</sub> and Li et al.<sup>[17]</sup> soaked the poly(2-acrylamido-2-methylpropanesulfonic acid)/polyacrylamide hydrogels in the LiCl-based ethylene glycol/water mixture. However, the solubility of most salts in organic solvents is lower than that in water and so the improvement in conductivity is limited. The other popular method is to introduce carbon-based conductive additives to the hydrogels. For instance, carbon nanotubes have been incorporated into the polyacrylamide/montmorillonite hydrogel<sup>[18]</sup> and the materials show conductivity of 10<sup>−6</sup>–10<sup>−7</sup> S cm<sup>−1</sup>, which is still 2–3 orders of magnitude lower than that of the original hydrogel. In our previous experiments, double network structures and sodium bonds (which are ionic bonds) are designed as stable charge channels to reduce the conductivity decrease of organohydrogels.<sup>[19]</sup> There is only one order of magnitude conductivity difference before and after glycerol immersion, indicating a potentially effective way to improve the conductivity of organohydrogels by the solvent replacement process.

The Hofmeister effect is a well-known concept based on the salt-in and salt-out properties, where salts influence many properties of proteins, gels, and aqueous solutions including the solubility and stability.<sup>[20,21]</sup> Therefore, in this work, the Hofmeister effect and electrostatic interaction are introduced to the double network hydrogels and studied systematically. To understand the potential impact of the Hofmeister effect on the

Y. Wu, Y. Mu, Z. Zhou, S.-P. Feng  
Department of Mechanical Engineering  
The University of Hong Kong  
Hong Kong 999077, China  
E-mail: hpfeng@hku.hk

Y. Wu, C. Menon  
Biomedical and Mobile Health Technology Lab  
Department of Health Sciences and Technology  
ETH Zurich  
Zurich 8008, Switzerland

Y. Luo, P. K. Chu  
Department of Physics  
Department of Materials Science and Engineering, and Department  
of Biomedical Engineering  
City University of Hong Kong  
Hong Kong 999077, China  
E-mail: yluo24-c@my.cityu.edu.hk

 The ORCID identification number(s) for the author(s) of this article can be found under <https://doi.org/10.1002/adfm.202110859>.

DOI: 10.1002/adfm.202110859

organohydrogel conductivity, the physical characteristics, such as microstructures and mechanical properties of sodium salt-based organohydrogels are analyzed and compared. The contribution of the chemical bond formed by electrostatic interaction to the organohydrogel conductivity is also investigated and the lithium and sodium bonds play more important roles than the common hydrogen bonds. Our study elucidates the synergistic enhancement mechanism of the Hofmeister effect and electrostatic interaction on the organohydrogel conductivity and is confirmed by the output of the corresponding triboelectric nanogenerators. The champion organohydrogel has also been demonstrated in other electronic applications including photovoltaic and thermoelectric devices.

## 2. Results and Discussion

There are empirical Hofmeister series for both anions and cations, while the anionic series plays a more important role.<sup>[22–24]</sup> Figure 1a presents the simplified anionic Hofmeister series, in which anions on the left-side ( $\text{SO}_4^{2-}$ ,  $\text{HPO}_4^{2-}$ , etc.) and right-side ( $\text{SCN}^-$ ,  $\text{ClO}_3^-$ , etc.) exhibit opposite phenomena (salting-out and salting-in), and therefore are considered as the kosmotropes (“structure maker”) and chaotropes (“structure breaker”), respectively.<sup>[23]</sup> To investigate the potential impact of the anionic Hofmeister series on the physical properties of the hydrogels, four commonly used salts with the same cation ( $\text{Na}^+$ ) but different anions ( $\text{SO}_4^{2-}$ ,  $\text{CO}_3^{2-}$ ,  $\text{Cl}^-$ ,  $\text{NO}_3^-$ ) are introduced to the polyacrylamide/poly(vinyl alcohol) (referred to as AV) organohydrogels using a glycerol immersion process. As shown

in Figure 1b, the microstructure of AV organohydrogels with different salts varies significantly, especially the cavity size that shows an increasing trend of  $\text{AV}/\text{Na}_2\text{SO}_4 < \text{AV}/\text{Na}_2\text{CO}_3 < \text{AV}/\text{NaCl} < \text{AV}/\text{NaNO}_3$ , following the generally accepted Hofmeister series. It is mainly because the salting-out phenomenon caused by salts such as  $\text{Na}_2\text{SO}_4$  makes it harder for hydrogels to generate cavities. In contrast, the salting-in phenomenon produced by salts, such as  $\text{NaNO}_3$  enables the hydrogels to produce more and bigger cavities (compared to the porous structure of the AV organohydrogel in Figure S1, Supporting Information).<sup>[24]</sup>

Moreover, it is important to explore how the Hofmeister effect affects the other properties of the above-mentioned organohydrogels, for example, the mechanical properties that are important to flexible and wearable devices, and the conductivity that is essential to electronic applications. As shown in Figure 1c; and Figure S2a (Supporting Information), except for AV/NaCl organohydrogel, the tensile strength and elongation at break of the other three organohydrogels are in a decreasing order of  $\text{AV}/\text{Na}_2\text{SO}_4 > \text{AV}/\text{Na}_2\text{CO}_3 > \text{AV}/\text{NaNO}_3$ , from 165.7 KPa and 1943.5% to 62.6 KPa and 1061.7%. It is noted that the mechanical properties of the AV/NaNO<sub>3</sub> organohydrogel is worse than that of the AV organohydrogel (Figure S2b, Supporting Information), because the salting-in property of  $\text{NO}_3^-$  plays a “structure breaker” role. On the other hand, it is assumed that the tensile strength and elongation at break of the AV/NaCl organohydrogel should follow the Hofmeister series tendency and the stress and strain values ideally should be around the range of the dotted circle in Figure 1c. However, the data “move” to the solid circle, showing a tensile strength of 126.7 KPa and elongation at break of 2224.2% that are higher

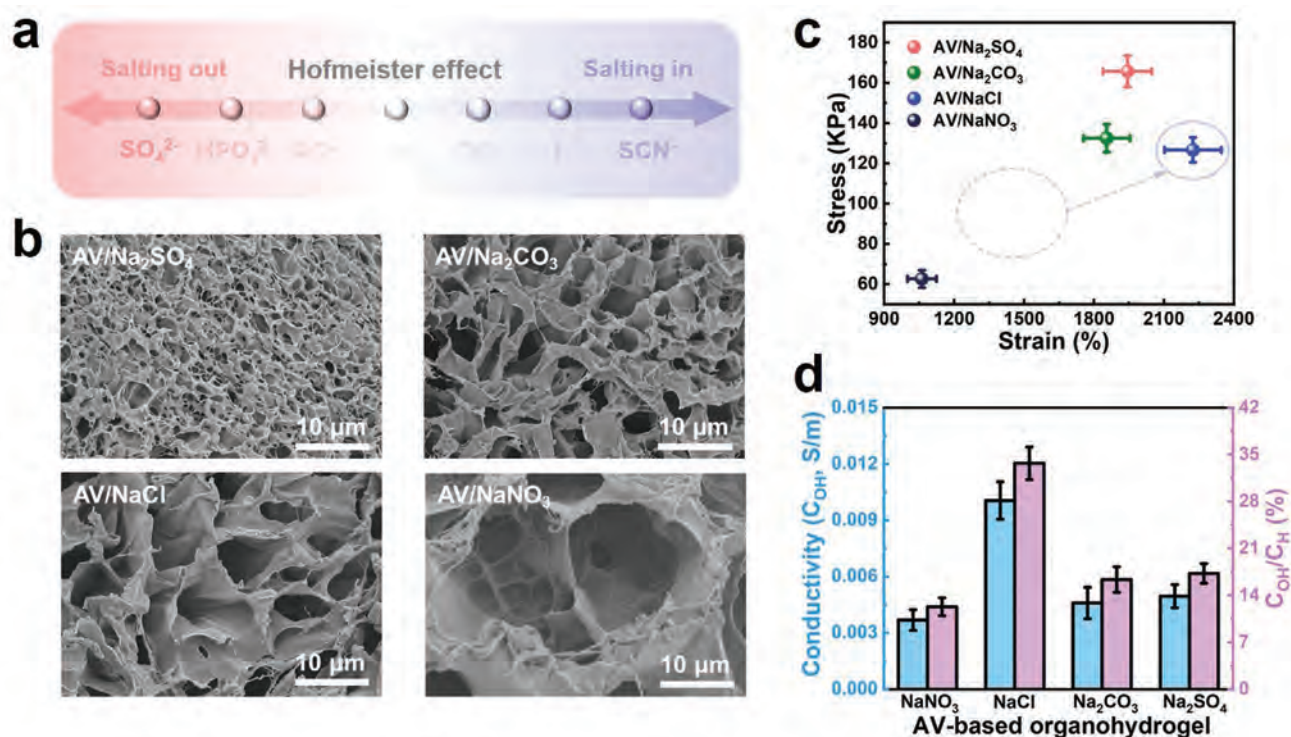


**Figure 1.** Impact of the Hofmeister effect on the AV-based organohydrogels: a) Schematic illustration of the simplified anionic Hofmeister series, b) SEM images, c) Stress and strain values, and d) Conductivity comparison of various sodium salt-based AV organohydrogels.

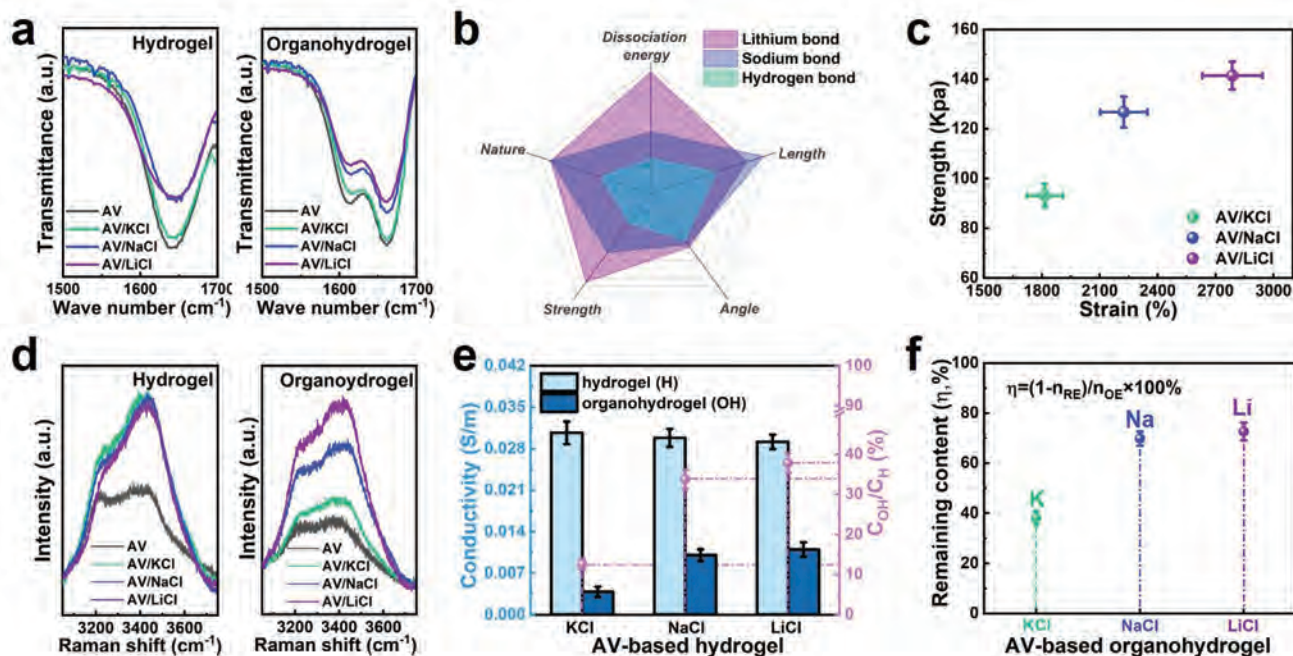


**Figure 2.** Impact of the electrostatic interaction on the AV-based organohydrogels: a) FTIR spectra of various chloride salt-based AV hydrogels/organohydrogels, b) Schematic comparison of various factors of the lithium, sodium, and hydrogen bonds, c) Stress and strain values, d) Raman scattering spectra and e) Conductivity of the chloride salt-based AV hydrogels/organohydrogels, and f) Remaining percentages of cations in the additive salts in the organohydrogels.

than expected, suggesting the involvement of other important effects (except for the Hofmeister effect) in the AV/NaCl system. It will be discussed later in this paper.

Considering its important role in electronic applications, the conductivity of the above-mentioned salt-based AV organohydrogels is further determined. Figure S3 (Supporting Information) shows similar conductivity values for these salt-based AV hydrogels due to the same concentration of the added sodium salts that are much higher than that of the pure AV hydrogel (control), revealing the significant contribution of sodium salts in the original hydrogels. However, after glycerol immersion, the conductivity of the organohydrogels decreases due to the excessive overflow of additive salts and the introduction of glycerol during the solvent replacement process. Interestingly, the conductivity of the AV/NaCl organohydrogel is 2–3 times larger than that of the AV/Na<sub>2</sub>SO<sub>4</sub>, AV/Na<sub>2</sub>CO<sub>3</sub>, and AV/NaNO<sub>3</sub> organohydrogels as shown in Figure 1d. Consequently, the remaining percentage of conductivity ( $C_{OH}/C_H$ , the ratio of organohydrogel and hydrogel conductivity) of the organohydrogels in the AV/NaCl system is also the highest (~34%) compared to the others of only 12–17%. This indicates again the dominant effect that contributes to the high conductivity of the AV/NaCl organohydrogel is no longer the Hofmeister effect but other factors, for instance, the sodium bonds described in our paper.<sup>[19]</sup>

Therefore, it is important to systematically study the potential electrostatic interaction occurring in the hydrogel synthesis process. Since both lithium and sodium bonds can be formed by electrostatic interaction,<sup>[25]</sup> LiCl, NaCl, and KCl are introduced to the AV systems. Compared to the AV hydrogel/organohydrogel in Figure 2a, no apparent peak difference at 1600–1700 cm<sup>-1</sup> is observed from the AV/KCl hydrogel/organohydrogel, indicating

that there no extra bonds generated after the addition of KCl. However, the obviously smaller peak intensity at ~1640 cm<sup>-1</sup> observed from both AV/NaCl and AV/LiCl hydrogels indicates that the sodium/lithium coordinative bonds may be formed between cations and coordinated carbonyl oxygen.<sup>[26,27]</sup> Similar phenomena are observed from the AV/NaCl and AV/LiCl organohydrogels, implying that the solvent replacement process is not able to break the sodium/lithium bonds.

Lithium and sodium bonds have similar bonding principles with hydrogen bonds. However, compared to the hydrogen bond, lithium and sodium bonds have several advantages as summarized in Figure 2b. First, the bonding nature of lithium and sodium bonds is mainly based on electrostatic interaction but hydrogen bonds are mainly based on the covalent interaction. Second, the dissociation energy order of the three bonds is lithium bond > sodium bond > hydrogen bond.<sup>[28,29]</sup> It is noted that the dissociation energy can be considered as one of the effective parameters to quantitatively describe the bond strength. The larger the dissociation energy, the stronger is the bond formed. Last but not least, even if taking other parameters such as bond energy and bond order into consideration, the bond strength of lithium and sodium bonds is still stronger than that of hydrogen bonds. Typically, the lithium bond is close to a chemical bond, the hydrogen bond is governed by van der Waals forces, and the sodium bond is somewhere in between. Therefore, it is reasonable that the stress and strain of the AV/LiCl and AV/NaCl organohydrogels in Figure 2c and Figure S4 (Supporting Information) are higher than those of the AV/KCl organohydrogel, even though these salts have the same anion that should show the similar Hofmeister effect (The cavity sizes of AV/LiCl and AV/KCl organohydrogels in

Figure S5 (Supporting Information) exhibit no appreciable difference compared to AV/NaCl organohydrogel).

As shown in Figure 2d, the Raman spectra of the AV, AV/KCl, AV/NaCl, and AV/LiCl hydrogels and organohydrogels reveal the presence of chloride salts. Compared to the pure AV hydrogel that exhibits two characteristic peaks ( $\approx 3215$  and  $\approx 3400$   $\text{cm}^{-1}$ ) of water molecules, the apparently larger peak intensity at  $3410\text{--}3430$   $\text{cm}^{-1}$  indicates OH stretching bonds of chloride salts in the salt-based AV hydrogels.<sup>[30]</sup> A similar peak intensity comes from the same concentration of added chloride salts. However, after glycerol immersion, the peak intensity of the three organohydrogels changes significantly in the order of AV/KCl < AV/NaCl < AV/LiCl. This means that the concentration of remaining chloride salts in the AV/LiCl organohydrogel is greater than that in the AV/NaCl organohydrogel, and both are much higher than that in the AV/KCl organohydrogel. Therefore, the three hydrogels have similar conductivity as shown in Figure 2e and Figure S6 (Supporting Information), while the corresponding organohydrogels show significant differences. For example, the remaining percentages of conductivity ( $C_{\text{OH}}/C_{\text{H}}$ ) in the organohydrogels are  $\approx 38\%$  and  $\approx 34\%$  for the AV/LiCl and AV/NaCl systems, respectively, but it is only  $\approx 13\%$  for the AV/KCl system. In comparison to the reported organohydrogels using the replacement method in Table S1 (Supporting Information), our developed AV/LiCl organohydrogel shows excellent conductivity, suggesting an important contribution of the Hofmeister effect and electrostatic interaction on the remaining conductivity of organohydrogels. More detailed discussion can be found in the Supporting Information.

In addition to compare the physical properties of organohydrogels, another way is to evaluate the content of cationic elements in the additive salts in the remaining glycerol after immersion. In this work, different chloride salt-based AV hydrogels are immersed in pure glycerol under the same immersion conditions. As shown in Table S2 (Supporting Information), the concentration of the cationic elements in the remaining glycerol varies greatly, even if the original concentration of the added salts is the same. Considering the different relative atomic masses of different elements, the remaining percentage of the measuring element in the organohydrogels is calculated by the equations in the supporting information and summarized in Figure 2f. The remaining percentage of lithium and sodium in AV/LiCl and AV/NaCl organohydrogels is almost twice as large as that of potassium in the AV/KCl organohydrogel. Therefore, it can be confirmed that most lithium and sodium bonds formed by electrostatic interaction still exist in the organohydrogels even after glycerol immersion. (Besides, the detailed discussion concerning nondrying and antifreezing properties of organohydrogels obtained by the solvent replacement method in this work can be found in the supporting information (Figure S7, Supporting Information).

It has been reported that  $\text{Na}^+$  exhibits a similar Hofmeister effect as  $\text{Cs}^+$ , while  $\text{Li}^+$  is similar to  $\text{Ca}^{2+}$  and  $\text{Mg}^{2+}$ .<sup>[24]</sup> Thus, the same concentration of  $\text{CsCl}$ ,  $\text{CaCl}_2$ , and  $\text{MgCl}_2$  salts is introduced to the AV hydrogels and compared with AV/NaCl and AV/LiCl systems in order to exclude the potential impact of the Hofmeister effect. Different from AV/NaCl and AV/LiCl systems, **Figure 3a** shows no obvious peak difference between AV/CsCl, AV/CaCl<sub>2</sub>, AV/MgCl<sub>2</sub>, and pure AV systems for both

hydrogels and organohydrogels. This indicates no additional bonds formation with the introduction of  $\text{CsCl}$ ,  $\text{CaCl}_2$ , and  $\text{MgCl}_2$  salts. As shown in Figure 3b, the chloride-based salts increase the peak intensity at  $3410\text{--}3440$   $\text{cm}^{-1}$  (OH stretching of chloride salts) compared to the AV hydrogel. However, after glycerol immersion, the peak intensity decreases dramatically to be slightly higher than or close to that of the pure AV organohydrogel. This indicates that a lot of chloride salts in AV/CsCl, AV/CaCl<sub>2</sub>, and AV/MgCl<sub>2</sub> organohydrogels are transferred to the glycerol solution during immersion.

More intuitive evidence is presented in Figure 3c and Table S3 (Supporting Information), where only around 37–40% of the cations (Cs, Ca, or Mg) remain in the AV/CsCl, AV/CaCl<sub>2</sub>, and AV/MgCl<sub>2</sub> organohydrogels. The results are similar to the remaining element (K) in the AV/KCl organohydrogel, but much lower than the remaining elements (Na or Li) in the AV/NaCl and AV/LiCl organohydrogels in Figure 2f. Further investigation on the remaining glycerol after chloride salt-based AV hydrogels immersion, the conductivity values in Table S4 (Supporting Information) indicate that, less LiCl and NaCl salts leave the original hydrogels under the same solvent replacement process. The lower conductivity indicates the less chloride salts remaining in the glycerol solutions, and further the more stable bonds between the cation and the carbonyl oxygen. Therefore, the lithium/sodium bond formed by the electrostatic interaction still plays a key role, even if they show the similar Hofmeister effect. In this case, as shown in Figure 3d that, the conductivity of the AV/CsCl, AV/CaCl<sub>2</sub>, and AV/MgCl<sub>2</sub> organohydrogels is much lower than that of AV/NaCl and AV/LiCl organohydrogels, although the original conductivity of the former hydrogels is similar to or even higher than that of the latter hydrogels.

Accordingly, an overall review of the impact of various ions on the conductivity of the organohydrogels by the solvent replacement method is summarized in Figure 3e and described as follows. First, the Hofmeister effect influences the conductivity of the organohydrogels. The salting-out phenomenon makes less and smaller cavities in the hydrogel and there is less transfer of salts from the hydrogel to the glycerol during immersion. Second, although cations are not as important as anions in the Hofmeister effect, the lithium and sodium bonds formed by the electrostatic interaction are key to the high conductivity of organohydrogels. Third, the electrostatic interaction plays a more important role than the Hofmeister effect in the remaining conductivity of organohydrogels using the solvent replacement method.

To confirm the aforementioned theory, the electronic applications of the salt-based AV organohydrogels are investigated. Owing to the flexibility, conductivity, and stability, the organohydrogels are considered as ionic conductors in single-electrode triboelectric nanogenerators (S-TENGs). As shown in **Figure 4a** and Figure S8 (Supporting Information), the organohydrogels are covered by silicone rubber (Ecoflex) films and a benzophenone treatment is performed to generate covalent bonds between the Ecoflex and organohydrogels to improve the mechanical reliability.<sup>[31]</sup> The working mechanism of S-TENGs can be found elsewhere<sup>[32,33]</sup> and alternating electronic signals are produced during the contact and separation cycles. The open-circuit voltage ( $V_{\text{OC}}$ ) of the AV/LiCl- and AV/NaCl-based S-TENGs in Figure 4b is larger than that of the AV/KCl- and

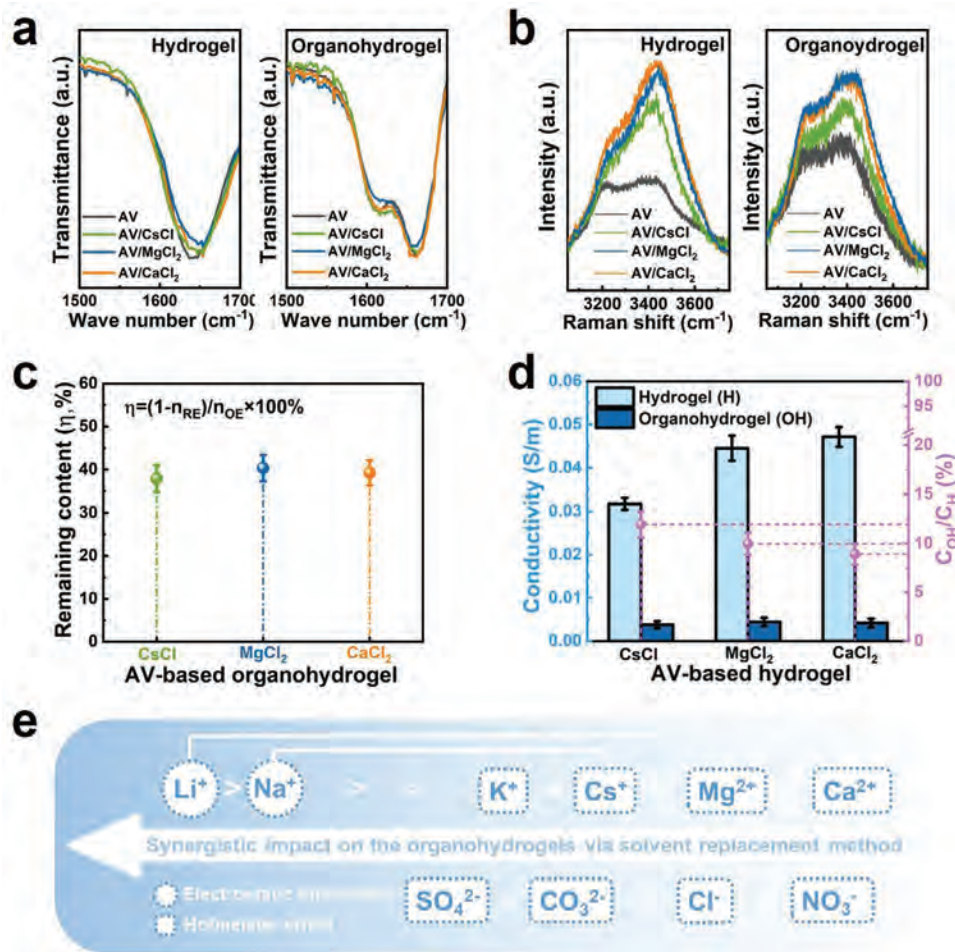


**Figure 3.** Synergistic effects on the AV-based organohydrogels: a) FTIR spectra, b) Raman scattering spectra, c) Remaining percentages of cations in the organohydrogels, and d) Conductivity of various chloride salts-based AV hydrogels/organohydrogels. e) Schematic summary of the synergistic effects on the conductivity of AV-based organohydrogels using the solvent replacement method.

AV-based S-TENGs, because the lithium and sodium bonds in these electrodes give rise to more stable charge channels and higher conductivity. The  $V_{OC}$  values in Figure 4c illustrate the impact of the Hofmeister effect and electrostatic interaction. For instance,  $V_{OC}$  shows a decreasing order from AV/ $\text{Na}_2\text{SO}_4^-$ , AV/ $\text{Na}_2\text{CO}_3^-$ , to AV/ $\text{NaNO}_3^-$ -based S-TENGs, proving that the salting-out property based on the Hofmeister effect can improve the conductivity of organohydrogels and the TENG output. However, the electrostatic interaction plays a more important role in the output consistent with the conductivity. Therefore, the output of the AV/ $\text{NaCl}$ -based S-TENG is higher than that of the AV/ $\text{CsCl}$ -based S-TENG, although these two organohydrogels show the similar salting-out effect. Meanwhile,  $V_{OC}$  of the AV/ $\text{LiCl}$ -based S-TENG is about twice that of those of the AV/ $\text{MgCl}_2^-$  and AV/ $\text{CaCl}_2^-$ -based S-TENGs with a similar Hofmeister effect. By considering the best performance, the short-circuit current density ( $J_{SC}$ ) and power density of AV/ $\text{LiCl}$  organohydrogel were measured and shown in Figure S9 (Supporting Information). Its overall output performance was further compared with reported works in Table S5 (Supporting Information) with detailed discussion in the Supporting Information.

Recently, the combination of triboelectric and photovoltaic effects has gained increasing attention.<sup>[34–37]</sup> It is common that a transparent TENG covers the surface of a solar cell (Figures S10a and S11, Supporting Information) to simultaneously harvest mechanical and solar energies. Considering the high transparency of the AV/ $\text{LiCl}$  organohydrogel (Figure S12, Supporting Information), a commercial Si-based solar cell is used to evaluate the potential effect of the transparent layer on its performance. The detailed data analysis (Figure S10 and Table S6, Supporting Information) and performance comparison with reported works (Table S7, Supporting Information) can be found in the Supporting Information.

Hydrogel is also widely used in thermoelectric applications.<sup>[38,39]</sup> Figure 4d shows the working principle of common hydrogel-based cells based on the temperature gradient between the two electrodes. Considering the stable charge channels and inorganic salts remaining in the organohydrogels, the thermopower of the AV/ $\text{LiCl}$  organohydrogel-based cell (Figure S13, Supporting Information) for thermoelectric applications is investigated. As shown in Figure 4e,f, the thermovoltage of the AV/ $\text{LiCl}$  organohydrogel-based cell increases with increasing

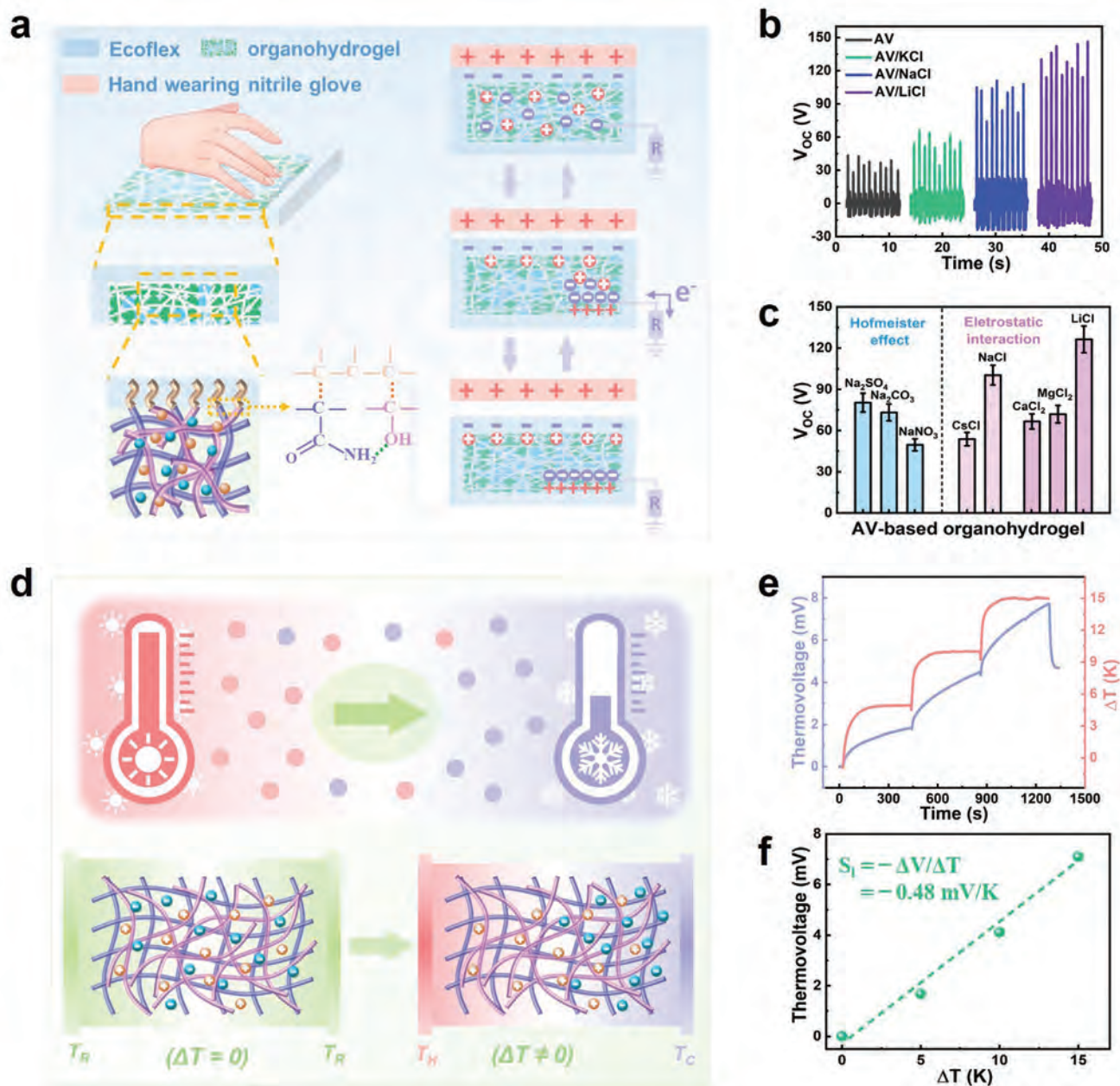


**Figure 4.** Electronic applications of the AV/LiCl organohydrogel: a) Schematic illustration of S-TENG fabrication and working principle, b)  $V_{OC}$  signals of various AV-based S-TENGs, and c)  $V_{OC}$  comparison of various AV-based S-TENGs based on the Hofmeister effect and electrostatic interaction. d) Schematic illustration of the working mechanism of the AV/LiCl organohydrogel-based cell based on thermodiffusion effect, and e, f) thermovoltage and thermopower of the AV/LiCl organohydrogel-based cell.

temperature difference between the cold and hot electrodes. A thermopower of  $-0.48 \text{ mV K}^{-1}$  is obtained and it is acceptable because no redox couples are involved and it is similar to the reported alkali halide solutions.<sup>[40]</sup> The negative thermopower arises from the movement of the anion ( $\text{Cl}^-$ ) from the hot electrode to the cold electrode (Figure 4d), because most of the remaining cations ( $\text{Li}^+$ ) in the organohydrogel are bonded to the chains via the electrostatic interaction. More detailed comparison with other works was summarized in Table S8 (Supporting Information).

### 3. Conclusion

In this work, the enhancement mechanism of the Hofmeister effect and electrostatic interaction on the conductivity of organohydrogels by solvent replacement is investigated. Compared to the salting-in phenomenon, the salting-out phenomenon based on the Hofmeister effect shows positive impact on the conductivity due to the formation of smaller cavities which avoid excessive transfer of inorganic salts from the hydrogels to glycerol solutions. The key factor affecting

the high conductivity of organohydrogels is the formation of lithium/sodium bonds by the electrostatic interaction. Owing to the stronger bonding, these bonds are stable in the organohydrogels even after the solvent replacement process. Thus, the organohydrogels can be used as ionic conductors and antireflective layers in electronic applications including triboelectric, photovoltaic, and thermoelectric devices. This work presents a promising approach to alleviate the conductivity decrease of organohydrogels by solvent replacement and the proposed mechanism is expected to advance the understanding of the contribution of ions to organohydrogels for electronic applications.

#### 4. Experimental Section

**Synthesis of Organohydrogel:** The organohydrogel was synthesized as described previously.<sup>[19]</sup> Typically, poly(vinyl alcohol) (PVA) (10 wt%) and inorganic salts (0.5–1 M) were dissolved in the deionized water at 95 and 25 °C, respectively. The salt solution, acrylamide (AM, 2 M), *N,N*-methylenebisacrylamide (MBA, 0.06 wt%), and ammonium persulfate (APS, 1 wt%) were dissolved sequentially in the cooled PVA solution. After pouring into a PTFE module, the mixture was illuminated by UV light at 365 nm. Following that, the as-prepared hydrogel was soaked in the pure glycerol solution and after removing the solvent with weighing paper, the organohydrogel was ready for further use.

**Fabrication of the organohydrogel-based S-TENG (OHS-TENG):** Similar to the previous work,<sup>[32]</sup> a typical OHS-TENG was fabricated by the following steps. First, a silicone rubber (Ecoflex) layer with a size of 2 × 2 cm<sup>2</sup> was prepared and underwent the benzophenone treatment. The mixture was poured into the Ecoflex holder and illuminated with UV light (365 nm). The hydrogel-based Ecoflex film was soaked in a pure glycerol solution and after attaching an Ag tape, the Ecoflex precursor was used to seal the organohydrogel and device edge. After curing at 80 °C for 2 h, the sandwiched OHS-TENG was fabricated.

**Characterization and Measurement:** A Fourier transform infrared spectrometer (FTIR, JASCO 6600) and Raman scattering spectrometer (LabRAM HR, HORIBA) were used to analyze the molecular structure of the samples. An ultraviolet and visible spectrophotometer (UV-vis, JENWAY, 6850) was used to measure the transmittance of the samples in the range of 400–800 cm<sup>-1</sup>. A scanning electron microscope (SEM, HITACHI, SU5000) was used to examine the surface morphology of the water-swelled and freezer-dried samples. A microcomputer controlled electronic universal testing machine (CMT6103, MTS) with a stretching speed of 100 mm min<sup>-1</sup> was used to conduct the mechanical properties of the samples. A potentiostat/galvanostat instrument (Autolab PGSTAT302N) and a METTLER TOLEDO were employed to measure the conductivity of the hydrogel samples and liquid solutions, respectively. An inductively-coupled plasma optical emission spectrometer (ICP-OES, Agilent 720ES) was used to determine the elemental concentration in the remaining glycerol solutions. A Keithley source meter (Model 2400) and oscilloscope (RIGOL DS1054Z) with a high voltage probe (RIGOL PR1050D, 100 MΩ), were utilized to evaluate the output of the triboelectric nanogenerators. A solar simulator (Pecell PECL01) with standard AM 1.5G light illumination (100 mW cm<sup>-2</sup>) was used to record the *J*-*V* curves of hybrid devices. An electrochemical workstation (Chenhua CHI660E) was used to conduct the thermovoltage of organohydrogel-based cells in which graphite foils were the electrodes and the working electrode was connected to the hot side.

#### Supporting Information

Supporting Information is available from the Wiley Online Library or from the author.

#### Acknowledgements

This work was supported by the General Research Fund of the Research Grants Council of Hong Kong Special Administrative Region, China under Award Nos. 17206519 and 17203520. This work was also partially supported by HKU-Zhejiang Institute of Research and Innovation (HKU-ZIRI), China, and City University of Hong Kong Strategic Research Grant, China, No. 7005505.

#### Conflict of Interest

The authors declare no conflict of interest.

#### Data Availability Statement

Research data are not shared.

#### Keywords

electronic applications, electrostatic induction, Hofmeister effect, organohydrogels, solvent replacement

Received: October 26, 2021

Revised: November 29, 2021

Published online: December 22, 2021

- [1] C.-C. Kim, H.-H. Lee, K. H. OH, J.-Y. Sun, *Science* **2016**, 353, 682.
- [2] B. Lee, H. Cho, K. T. Park, J.-S. Kim, M. Park, H. Kim, Y. Hong, S. Chung, *Nat. Commun.* **2020**, 11, 5948.
- [3] D. Gao, K. Parida, P. S. Lee, *Adv. Funct. Mater.* **2020**, 30, 1907184.
- [4] X. Liu, J. Liu, S. Lin, X. Zhao, *Mater. Today* **2020**, 36, 102.
- [5] Y. Cai, J. Shen, C.-W. Yang, Y. Wan, H.-L. Tang, A. A. Aljarb, C. Chen, J.-H. Fu, X. Wei, K.-W. Huang, Y. Han, S. J. Jonas, X. Dong, V. Tung, *Sci. Adv.* **2020**, 6, eabb5367.
- [6] Y. Cheng, K. H. Chan, X.-Q. Wang, T. Ding, T. Li, X. Lu, G. W. Ho, *ACS Nano* **2019**, 13, 13176.
- [7] J. H. Kim, K. G. Cho, D. H. Cho, K. Hong, K. H. Lee, *Adv. Funct. Mater.* **2021**, 31, 2010199.
- [8] C. Keplinger, J.-Y. Sun, C. C. Foo, P. Rothmund, G. M. Whitesides, Z. Suo, *Science* **2013**, 341, 984.
- [9] S. Park, K. Parida, P. S. Lee, *Adv. Energy Mater.* **2017**, 7, 1701369.
- [10] X. Liu, Q. Zhang, G. Gao, *ACS Nano* **2020**, 14, 13709.
- [11] Q. Rong, W. Lei, L. Chen, Y. Yin, J. Zhou, M. Liu, *Angew. Chem., Int. Ed.* **2017**, 56, 14159.
- [12] F. Chen, D. Zhou, J. Wang, T. Li, X. Zhou, T. Gan, S. H.-Wang, X. Zhou, *Angew. Chem., Int. Ed.* **2018**, 57, 6568.
- [13] J. Wu, Z. Wu, H. Xu, Q. Wu, C. Liu, B.-R. Yang, X. Gui, X. Xie, K. Tao, Y. Shen, J. Miao, *Mater. Horiz.* **2019**, 6, 595.
- [14] H. Chen, J. Huang, J. Liu, J. Gu, J. Zhu, B. Huang, J. Bai, J. Guo, X. Yang, L. Guan, *J. Mater. Chem. A* **2021**, 9, 23243.
- [15] B. Liu, F. Li, P. Niu, H. Li, *ACS Appl. Mater. Interfaces* **2021**, 13, 21822.
- [16] J. Song, S. Chen, L. Sun, Y. Guo, L. Zhang, S. Wang, H. Xuan, Q. Guan, Z. You, *Adv. Mater.* **2020**, 32, 1906994.
- [17] X. Li, D. Lou, H. Wang, X. Sun, J. Li, Y.-N. Liu, *Adv. Funct. Mater.* **2020**, 30, 2007291.
- [18] H. Sun, Y. Zhao, S. Jiao, C. Wang, Y. Jia, K. Dai, G. Zheng, C. Liu, P. Wan, C. Shen, *Adv. Funct. Mater.* **2021**, 31, 2101696.
- [19] Y. Wu, J. Qu, X. Zhang, K. Ao, Z. Zhou, Z. Zheng, Y. Mu, X. Wu, Y. Luo, S.-P. Feng, *ACS Nano* **2021**, 15, 13427.

- [20] P. Jungwirth, P. S. Cremer, *Nat. Chem.* **2014**, *6*, 261.
- [21] R. S. Carnegie, C. L. D. Gibb, B. C. Gibb, *Angew. Chem., Int. Ed.* **2014**, *53*, 11498.
- [22] S. Nihonyanagi, S. Yamaguchi, T. Tahara, *J. Am. Chem. Soc.* **2014**, *136*, 6155.
- [23] B. C. Gibb, *Nat. Chem.* **2019**, *11*, 963.
- [24] S. Wu, M. Hua, Y. Alsaied, Y. Du, Y. Ma, Y. Zhao, C.-Y. Lo, C. Wang, D. Wu, B. Yao, J. Strzalka, H. Zhou, X. Zhu, X. He, *Adv. Mater.* **2021**, *33*, 2007829.
- [25] S. Chen, J. Ishii, S. Horiuchi, M. Yoshizawa-Fujita, E. I. Izgorodina, *Phys. Chem. Chem. Phys.* **2017**, *19*, 17366.
- [26] B. Yiming, Y. Han, Z. Han, X. Zhang, Y. Li, W. Lian, M. Zhang, J. Yin, T. Sun, Z. Wu, T. Li, J. Fu, Z. Jia, S. Qu, *Adv. Mater.* **2021**, *33*, 2006111.
- [27] Z.-F. Li, Y.-C. Zhu, H.-X. Liu, *Phys. Chem. Chem. Phys.* **2009**, *11*, 11113.
- [28] Z. Li, X. Zhang, H. Li, Y. Zhu, X. Yang, *Chem. Phys. Lett.* **2011**, *510*, 273.
- [29] S.-J. Wang, Y. Li, D. Wu, Z.-R. Li, *Mol. Phys.* **2012**, *110*, 3053.
- [30] Q. Sun, *Vib. Spectrosc.* **2012**, *62*, 110.
- [31] H. Yuk, T. Zhang, G. A. Parada, X. Loi, X. Zhao, *Nat. Commun.* **2016**, *7*, 12028.
- [32] Y. Wu, Y. Luo, J. Qu, W. A. Daoud, T. Qi, *Nano Energy* **2020**, *75*, 105027.
- [33] J. Zhu, Y. Cheng, S. Hao, Z. L. Wang, N. Wang, X. Cao, *Adv. Funct. Mater.* **2021**, *31*, 2100039.
- [34] Y. Liu, N. Sun, J. Liu, Z. Wen, X. Sun, S.-T. Lee, B. Sun, *ACS Nano* **2018**, *12*, 2893.
- [35] Y. Cho, S. Lee, J. Hong, S. Pak, B. Hou, Y.-W. Lee, J. E. Jang, H. Im, J. I. Sohn, S. Cha, J. M. Kim, *J. Mater. Chem. A* **2018**, *6*, 12440.
- [36] Y. Wu, J. Qu, P. K. Chu, D.-M. Shin, Y. Luo, S.-P. Feng, *Nano Energy* **2021**, *89*, 106376.
- [37] Z. Ren, Q. Zheng, H. Wang, H. Guo, L. Miao, J. Wan, X. Chen, S. Cheng, H. Zhang, *Nano Energy* **2020**, *67*, 104243.
- [38] C.-G. Han, X. Qian, Q. Li, B. Deng, Y. Zhu, Z. Han, W. Zhang, W. Wang, S.-P. Feng, G. Chen, W. Liu, *Science* **2020**, *368*, 1091.
- [39] B. Guo, Y. Hoshino, F. Gao, K. Hayashi, Y. Miura, N. Kimizuka, T. Yamada, *J. Am. Chem. Soc.* **2020**, *142*, 17318.
- [40] S. D. Lecce, F. Bresme, *J. Phys. Chem. B* **2018**, *122*, 1662.



## Supporting Information

for *Adv. Funct. Mater.*, DOI: 10.1002/adfm.202110859

Hofmeister Effect and Electrostatic Interaction Enhanced  
Ionic Conductive Organohydrogels for Electronic  
Applications

*Yinghong Wu, Yijie Mu, Yang Luo,\* Carlo Menon,  
Zhiwen Zhou, Paul K. Chu, and Shien-Ping Feng\**

# **The Hofmeister Effect and Electrostatic Interaction Enhanced Ionic Conductive Organohydrogels for Electronic Applications**

*Yinghong Wu, Yijie Mu, Yang Luo\*, Carlo Menon, Zhiwen Zhou, Paul K. Chu, and Shien-Ping Feng\**

(Declaration of interest: none)

Dr. Y. Wu, Y. Mu, Dr. Z. Zhou, Prof. S.-P. Feng

Department of Mechanical Engineering, The University of Hong Kong, Hong Kong, China.

E-mail: [hpfeng@hku.hk](mailto:hpfeng@hku.hk)

Dr. Y. Wu and Prof. C. Menon

Biomedical and Mobile Health Technology Lab, Department of Health Sciences and Technology, ETH Zurich, Zurich, Switzerland.

Dr. Y. Luo and Prof. P. K. Chu

Department of Physics, Department of Materials Science and Engineering, and Department of Biomedical Engineering, City University of Hong Kong, Hong Kong, China.

E-mail: [ylo24-c@my.cityu.edu.hk](mailto:ylo24-c@my.cityu.edu.hk)

Dr. Y. Luo

Empa, ETH Domain, Dübendorf, Switzerland.

## Impact of the Hofmeister effect on the AV-based organohydrogels

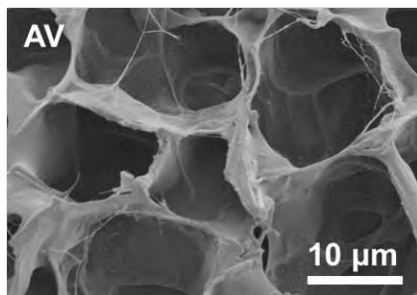


Figure S1. SEM image of the pure AV organohydrogel.

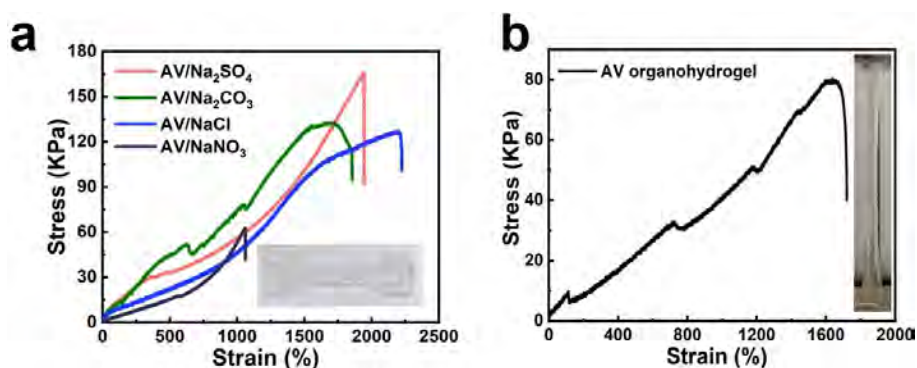
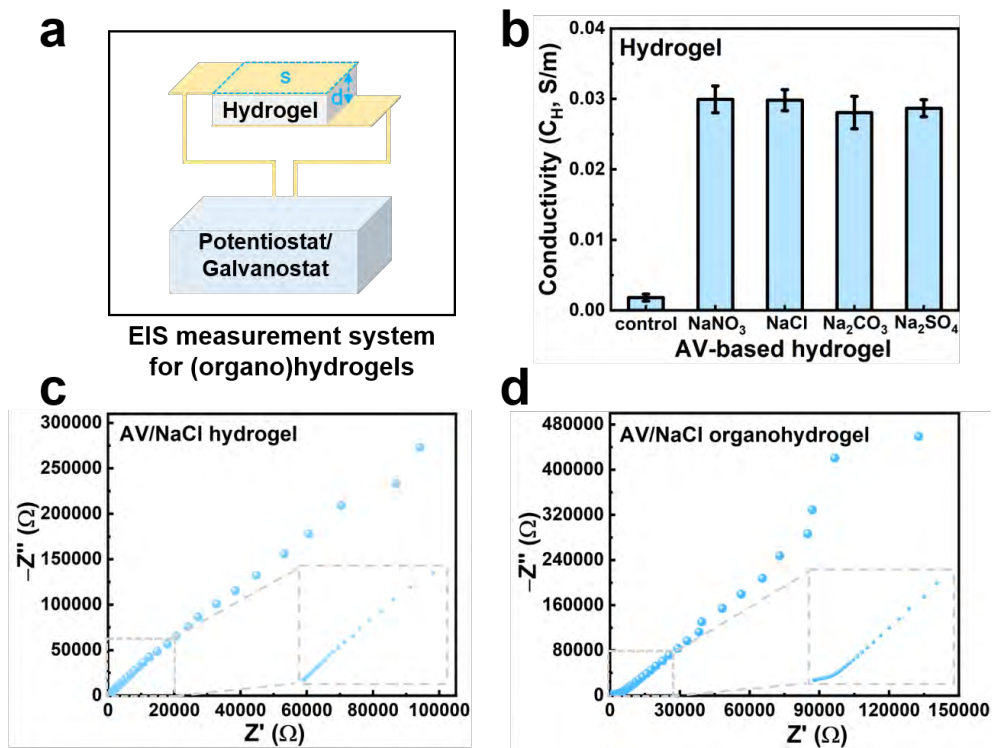


Figure S2. Mechanical properties of different AV-based organohydrogels. a) sodium salt-based AV organohydrogels, and b) pure AV organohydrogel. The samples for the stress-strain test were prepared in a standard dumbbell-shape PTFE mold.

The hydrogels/organohydrogels were prepared in a cuboid-shape PTFE mold. As shown in Figure S3a, the as-prepared samples were sandwiched by two Ag tapes connecting to a potentiostat/galvanostat instrument for the electrochemical impedance spectroscopy (EIS) measurement. In this case, the thickness ( $d$ ) of the sample is considered as the length between two electrodes, and the area ( $S$ ) is the surface area of the sample that was attached to the electrode. Therefore, the conductivity of the sample can be calculated by the following equation:

$$C = d/(R \cdot S)$$



**Figure S3. Conductivity of AV-based hydrogels/organohydrogels.** a) Schematic diagram of the EIS measurement system. b) conductivity of AV-based hydrogels. c,d) the Nyquist plots of AV/NaCl hydrogel/organohydrogel.

### Impact of electrostatic interaction on the AV-based organohydrogels

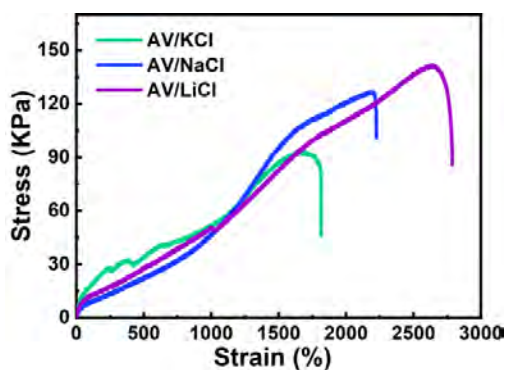


**Figure S4. Mechanical properties of different chloride salt-based AV organohydrogels.**

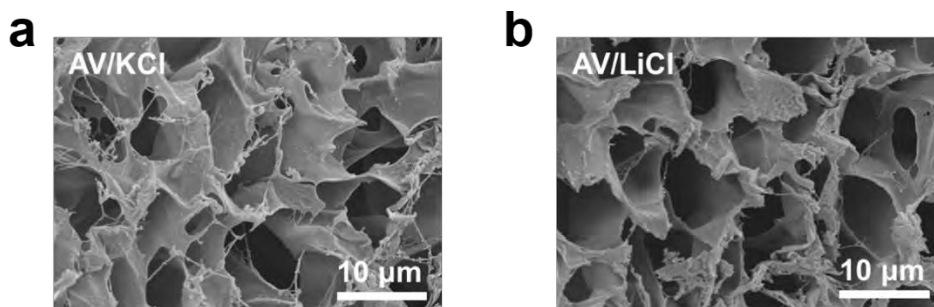


Figure S5. SEM images of AV/KCl and AV/LiCl organohydrogels.

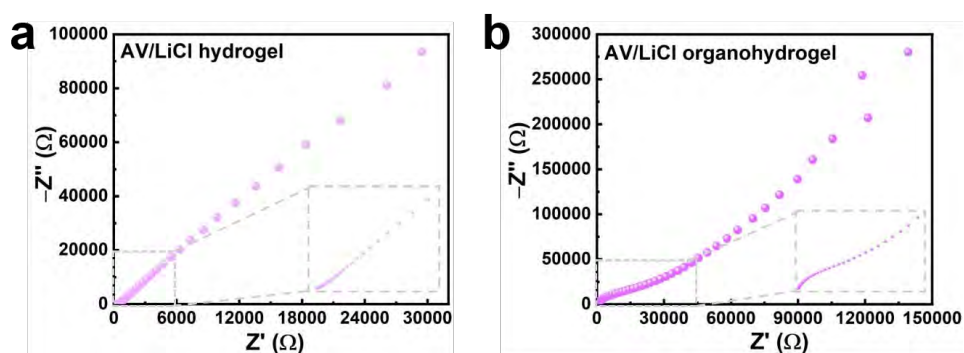


Figure S6. Nyquist plots of AV/LiCl hydrogels/organohydrogels.

### *Conductivity comparison with reported organohydrogels using the same method*

To fairly and comprehensively compare the conductivity of our developed organohydrogel with previous reported organohydrogels using the same solvent replacement method, the developed AV/LiCl organohydrogels in this work were immersed in pure glycerol, glycerol/water, or 1M LiCl/glycerol/water systems, respectively. As summarized in Table S1, when immersing in the pure glycerol, the conductivity of our organohydrogel is dozens of times that of the reported PAM/MMT/CNTs organohydrogel<sup>[18]</sup> and comparable to the PVA/Mxene/borax<sup>[S1]</sup>. Similarly, the conductivity of our AV/LiCl system is still as 20 times high as that of reported PAM/nano-clays system<sup>[S2]</sup>, after immersing these systems into the glycerol/water mixture. The conductivity of the reported PAM/carrageenan/KCl

organohydrogel<sup>[S3]</sup> was not given, probably because of the high resistance leading to the undetectable conductivity. Moreover, even if the replacement solvent is the mixture of salt, glycerol and water, the conductivity of the developed AV/LiCl organohydrogel in this work is still better than almost all other reported organohydrogels<sup>[16,17,S4-S12]</sup>. Therefore, it is indicated that the Hofmeister effect and electrostatic interaction are of great importance to improve the conductivity of organohydrogels through the solvent replacement method.”

**Table S1.** Conductivity comparison with reported organohydrogels using the solvent replacement method.

Ref.	Organohydrogel	Replacement solvent	Conductivity (S/m)
<b>This work</b>	PAM/PVA/LiCl	glycerol	0.011
[18]	PAM/MMT/CNTs	glycerol	0.0002~0.0003
[S1]	PVA/Mxene/borax	glycerol	0.005~0.045
<b>This work</b>	PAM/PVA/LiCl	glycerol/water	0.036
[S2]	PAM/nano-clays	glycerol/water	0.0015
[S3]	PAM/carrageenan/KCl	glycerol/ or ethylene glycol/water	N.A.
<b>This work</b>	PAM/PVA/LiCl	1M LiCl/glycerol/water	2.52
[16]	PEGDA/SA	0.5M KCl/0.023 M CaCl <sub>2</sub> /glycerin/water	0.756
[17]	PAMPS/PAM	4M LiCl/ethylene glycol/water	2.29
[S4]	xanthan gum/PAM	0.1M FeCl <sub>3</sub> glycerol/water	0.047~0.27
[S5]	PDA-rGO/SA/PAM	0.3M CaCl <sub>2</sub> glycerol/water	1.94
[S6]	PVA/SA	1M CaCl <sub>2</sub> glycerol/water	1.69
[S7]	HP-cellulose/PVA	2M LiClO <sub>4</sub> glycerol/water	2.73
[S8]	gelatin/PAA/FeCl <sub>3</sub>	2M NaCl glycerol/water	>0.7
[S9]	gelatin	20wt% Na <sub>3</sub> Cit glycerol/water	0.47
[S10]	PVA/PAM/Zn <sub>2</sub> SO <sub>4</sub>	0.5M Zn <sub>2</sub> SO <sub>4</sub> /ethylene glycol/water	0.44
[S11]	Cellulose/BzMe <sub>3</sub> NOH	2.5M NaCl ethylene glycol/water	1.92
[S12]	Cellulose/BzMe <sub>3</sub> NOH	1-3M NaCl ethylene glycol/water	0.72-1.08

**Table S2.** ICP-OES results of the element content (Li, Na, K) in the glycerol solution after immersion.

Hydrogel	Measuring element	Weight concentration ( $C_W$ )
AV/LiCl	Li	126.85 mg/kg
AV/NaCl	Na	462.87 mg/kg
AV/KCl	K	1610.95 mg/kg

*Note: The glycerol solution was treated as inorganic solution before the ICP-OES measurement.*

*Calculation of the remaining element in the organohydrogel:*

(1) The content of the measuring element in the original hydrogel ( $n_{OE}$ , mol):

$$n_{OE} = n_S \times M_E / M_S$$

where  $n_S$ ,  $M_E$  and  $M_S$  represent the content of additive salt in the hydrogel, the relative atomic mass of the measuring element, and the relative molecular mass of the additive salt, respectively.

(2) The content of the measuring element in the immersed glycerol ( $n_{RE}$ , mol):

$$n_{RE} = C_W \times m_G / M_E$$

where  $C_W$  and  $m_G$  represent the weight concentration in the remaining glycerol and the weight of the immersed glycerol, respectively.

(3) The remaining percentage of the measuring element in the organohydrogel ( $\eta$ , %):

$$\eta = (1 - n_{RE}) / n_{OE} \times 100\%$$

### **Non-drying and anti-freezing properties of the AV-based organohydrogels**

To verify its non-drying and anti-freezing properties, the developed AV/LiCl organohydrogel with glycerol immersion was stored together with its corresponding hydrogel under different conditions (for instance, ambient condition for non-drying property and freeze dryer condition for anti-freezing property). As shown in Figure S7a, the AV/LiCl hydrogel gets dried and loses its flexibility only after one day storage at 25 °C under ambient condition. However, the AV/LiCl

organohydrogel in Figure S7b maintains its high flexibility even after 5 months storage under the same condition. On the other hand, the AV/LiCl hydrogel in Figure S7c gets dried and rigid soon after storing in the freeze dryer at -50 °C for 4 hours. However, its corresponding organohydrogel in Figure S7d keeps the outstanding flexibility even after 4 days storage under the same condition. This demonstrates an excellent non-drying and anti-freezing properties of the developed organohydrogels using solvent replacement process.

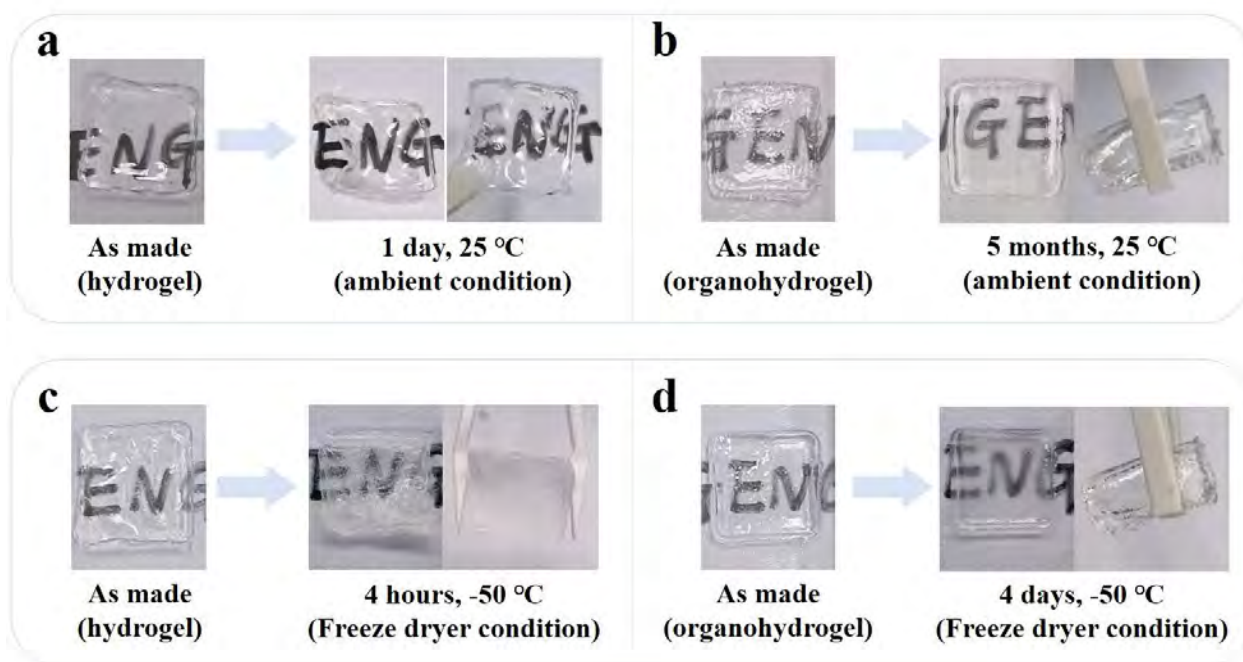


**Figure S7.** Comparison of (a, c) AV-based hydrogel and (b, d) organohydrogel under ambient condition (a, b) and freeze dryer condition (c, d).

### Impact of synergistic effect on the AV-based organohydrogels

**Table S3.** ICP-OES results of the element content (Cs, Mg, Ca) in the glycerol solution after immersion.

Hydrogel	Measuring element	Weight concentration ( $C_W$ )
AV/CsCl	Cs	5506.54 mg/kg
AV/MgCl <sub>2</sub>	Mg	966.81 mg/kg
AV/CaCl <sub>2</sub>	Ca	1624.44 mg/kg

*Note: The glycerol solution was treated as inorganic solution before the ICP-OES measurement.*



**Table S4.** Conductivity of the remaining glycerol after immersing different salt-based hydrogels.

Immersing hydrogel	Conductivity of the remaining glycerol ( $\mu\text{S}/\text{cm}$ )
/	0.00 (pure glycerol)
AV	0.57
AV/LiCl	22.0
AV/NaCl	25.2
AV/KCl	57.5
AV/CsCl	55.9
AV/MgCl <sub>2</sub>	54.3
AV/CaCl <sub>2</sub>	58.4

### Triboelectric applications of the AV-based organohydrogels



**Figure S8.** Photographs of the AV/LiCl organohydrogel-based TENG and its contact and separation with nitrile glove for output measurement.

As shown in Figure 4c and Figure S9, the developed AV/LiCl-based TENG in this work shows a  $V_{OC}$  of  $\sim 127$  V,  $J_{SC}$  of  $\sim 2.95$  mA/m<sup>2</sup>, and power density of  $\sim 302$  mW/m<sup>2</sup>, with a small device size of  $2 \times 2$  cm<sup>2</sup>. In comparison to other reported organohydrogel-based TENGs as summarized in Table S5, our developed device shows a competitive performance. Further comparing with those original hydrogel-based TENGs, the output of our AV/LiCl-based TENG is still better than most of these hydrogel-based TENGs without organic solvent replacement. This indicates the high performance of the developed device, apart from its excellent anti-freezing and anti-drying properties.

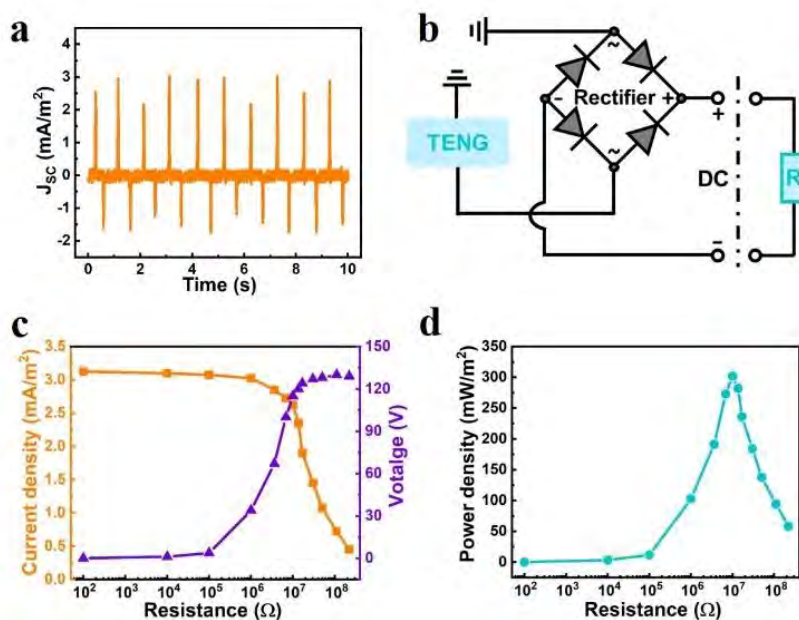


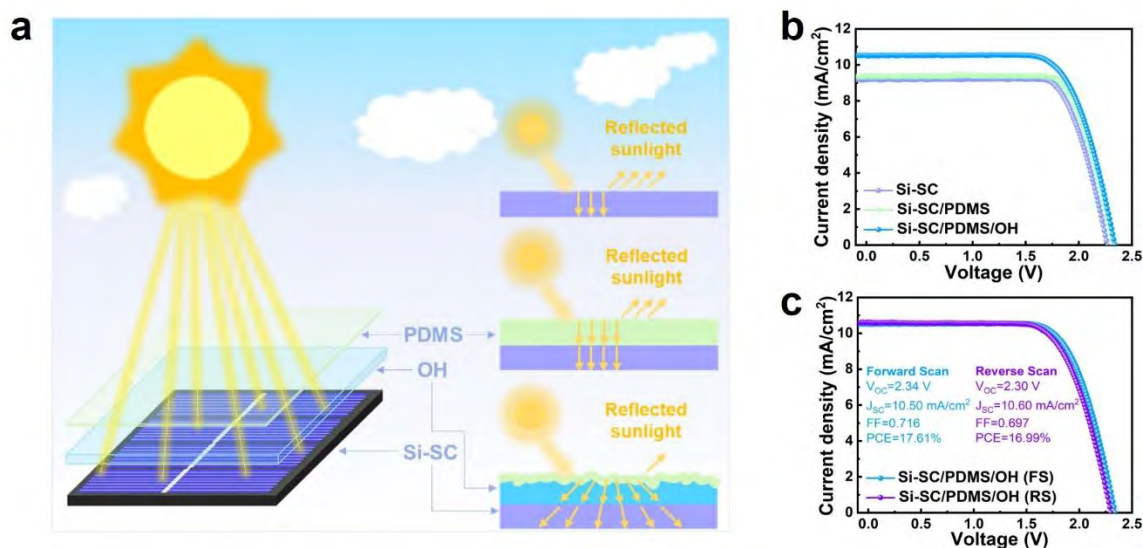
Figure S9. Current density and power density of AV/LiCl-based OH-TENGs.

Table S5. Performance comparison with reported organohydrogel/hydrogel-based TENGs.

Ref.	Organohydrogel (solvent replacement)	Electrode size (cm <sup>2</sup> )	V <sub>OC</sub> (V)	J <sub>SC</sub> (mA/m <sup>2</sup> )	power density (mW/m <sup>2</sup> )
This work	AV/LiCl	2×2	127	2.95	302
[18]	PAM/MMT/CNTs	4×3	86.4	0.92	41.2
[S2]	PAM/nano-clays	3×3	86	0.84	74.5
[S11]	Cellulose/BzMe <sub>3</sub> NOH	3×3	205	1.11	/
[S12]	Cellulose/BzMe <sub>3</sub> NOH	2×2	120	2.37	315
[S13]	PAM/Clay	4×4	157	10	710
Ref.	Hydrogel (No solvent replacement)	Electrode size (cm <sup>2</sup> )	V <sub>OC</sub> (V)	J <sub>SC</sub> (mA/m <sup>2</sup> )	power density (mW/m <sup>2</sup> )
[S14]	PVA	8×8	200	3.52	312.5
[S15]	PAM/LiCl	3×4	145	1.25	35
[S16]	PAM/SA	2×1	70	2.3	135
[S17]	PVA/PDA/CNTs/borax	3×3	95	1.11	750
[S18]	catechol-chitosan-diatom	3×3	110	4.2	29.8
[S19]	PAA/SA/Zn <sub>2</sub> SO <sub>4</sub>	4×1	30	1.25	32
[S20]	Mxene/PVA	2×5	230	0.27	330

## Photovoltaic applications of the AV/LiCl-based organohydrogels

As shown in the Figure S10b and Table S6, the bare solar cell exhibits an average short-circuit current density ( $J_{SC}$ ) of  $9.02 \text{ mA/cm}^2$ , open-circuit voltage ( $V_{OC}$ ) of  $2.23 \text{ V}$ , and power conversion efficiency (PCE) of  $15.39\%$ , which are slightly lower than those of the PDMS covered solar cell. It indicates that coverage of PDMS on the solar cell does not undermine the output due to the high transparency of PDMS (Figure S12). A transparent PDMS/LiCl/AV organohydrogel (OH) layer that is also a S-TENG is put on the solar cell. The characteristics of the PDMS/OH covered solar cell are further improved to  $10.22 \text{ mA/cm}^2$  for  $J_{SC}$ ,  $2.32 \text{ V}$  for  $V_{OC}$  and  $17.11\%$  for PCE, respectively. It is mainly because the PDMS/OH S-TENG has as an anti-reflected layer. As shown in the right patterns in Figure S10a, some sunlight is reflected from the bare and PDMS covered solar cell. Most of the reflected sunlight is absorbed by the PDMS/OH layer because the flexible organohydrogels and the bonds at the TENG interface result in an uneven surface.<sup>[31,37]</sup> Thus, the AV/LiCl-based TENG works as an anti-reflection layer for the Si-based SC, which effectively increases its PCE by  $1.72\%$ . Similar enhancement mechanism can also be found in other reported works as shown in Table S7, but the improved efficiency is normally not higher than  $1\%$ .<sup>[36, S22,S23,S27]</sup> On the other hand, there are many reported TENGs even show a negative impact on the performance of SCs, mostly because of the reduced transparency resulting from the coverage of TENGs.<sup>[S21,S24-S26]</sup> Moreover, negligible hysteresis is shown in Figure S10c, indicating good stability of the Si-based solar cell when covered by a PDMS/OH S-TENG. Therefore, it is promising to develop organohydrogels for hybrid photovoltaic-triboelectric devices.



**Figure S10.** (a) Schematic illustration of the combination of TENGs and solar cells and anti-reflection mechanism of the organohydrogels, (b, c) J-V curves of commercial Si-based solar cells covered with different layers

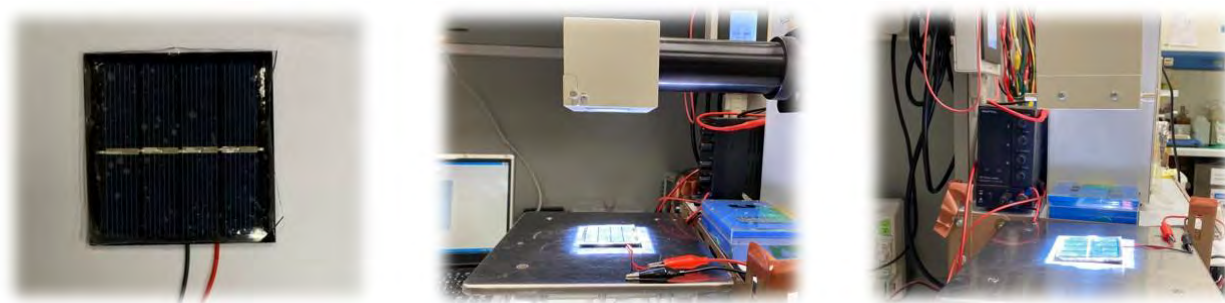


**Figure S11.** Photographs of the combination of AV/LiCl organohydrogel-based TENG and commercial silicon solar cell and its set-up for J-V curve measurement.

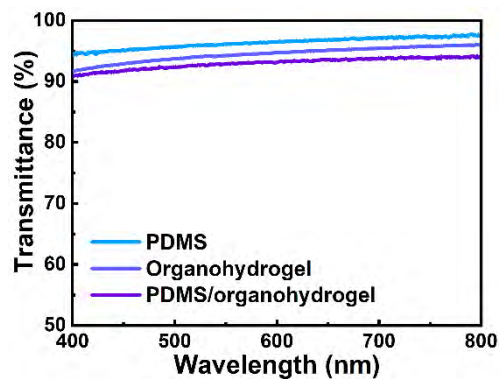


**Figure S12.** Optical transparency of various films. Transmittance spectra of PDMS (thickness:  $\sim 0.2$  mm), AV/LiCl organohydrogel (thickness:  $\sim 0.5$  mm), and PDMS-AV/LiCl organohydrogel (thickness:  $\sim 0.7$  mm) thin films.

**Table S6.** Summary of the photovoltaic parameters of commercial Si-based solar cells (SC) with or without PDMS and/or organohydrogel (OH).

Samples	$J_{SC}$ (mA/cm <sup>2</sup> )	$V_{OC}$ (V)	FF	PCE (%)
SC	9.03±0.15	2.23±0.11	0.74±0.02	15.39±0.41
SC/PDMS	9.15±0.13	2.30±0.04	0.73±0.04	16.30±0.23
SC/PDMS/OH	10.22±0.35	2.32±0.05	0.74±0.03	17.11±0.59

**Table S7.** Comparison of the effect of TENG on PCE of SC with reported works.

Ref.	TENG	Solar cell (SC)	Effect of TENG on PCE of SC
<b>This work</b>	AV-LiCl/Ecoflex	Commercial Si-SC	Increase from 15.39% to 17.11%
[36]	ITO/MNS-PDMS	+Al/P3HT:PC <sub>60</sub> BM/MoO <sub>3</sub>	Increase from 2.89% to 3.29%
[S21]	ITO/PDMS	Commercial SC	Decrease from 18.9% to 18.4%
[S22]	PVA-PEI-CDs/FEP	Commercial Si-SC	Increase from 13.6% to 14.6%
[S23]	Ag-ITO/NW-PDMS	+Si absorption layer/Al	Increase from 12.55% to 13.57%
[S24]	PET/ITO/PTFE	Si-based SC	Decrease from 16% to 14%
[S25]	ITO/PDMS-ITO/SiN	Si micropyramid SC	Decrease from 16% to 14%
[S26]	ITO/ZnO NWs-PDMS/ITO	DSSC	Decrease from 7.36% to 6.06%
[S27]	Ag-ITO/SiO <sub>2</sub>	+Si absorption layer/Al	Increase from 15.17% to 15.71%

### Thermoelectric applications of the AV/LiCl-based organohydrogels

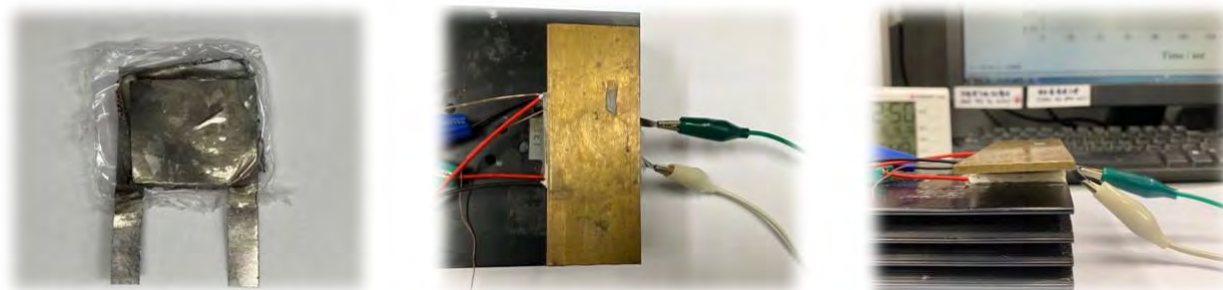


**Figure S13.** Photographs of the AV/LiCl organohydrogel-based thermoelectric cell and its set-up for thermovoltage measurement.

Compared to the reported works with the similar material systems (inorganic salt-based gels/polymers) or the same thermoelectric mechanism (the thermodiffusion of  $\text{Cl}^-$ ) as summarized in Table S8, the thermopower obtained by this work is in the middle level, which is closer to the high value. Therefore, the thermoelectric performance of our developed AV/LiCl-based cell is still acceptable and can be considered for future improvement and usage in thermoelectric applications.

**Table S8.** Performance comparison with reported thermoelectric cells based on inorganic salt-based gels/polymers or via the thermodiffusion of  $\text{Cl}^-$ .

Ref.	Thermoelectric cell	Thermopower (mV/K)
<b>This work</b>	graphite AV-LiCl graphite	-0.48
[S28]	Au EG-PEDOT:PSS Au	0.06~0.07
[S29]	SiNx/Au PEDOT-Tos SiNx/Au	0.023~0.26
[S30]	Au/Cr  $\text{Fe}(\text{CN})_6^{3-/4-}$ -PVA Au/Cr	1.02
[S31]	Pt  $\text{K}_3[\text{Fe}(\text{CN})_6]$ / $\text{K}_4[\text{Fe}(\text{CN})_6$ -agar] Pt	-1.09
[S32]	Au Cl-doped $\text{Cu}_3\text{SbS}_4$  Au	0.248~0.272
[S33]	Cu SWCNT/ADLA4 Cu	-0.067
[S34]	Pt  $\text{FeCl}_3$ -P3HT Pt	-2.7

## Reference

- [S1] H. Liao, X. Guo, P. Wan, G. Yu, *Adv. Funct. Mater.* **2019**, *29*, 1904507.  
[S2] Z. Xu, F. Zhou, H. Yan, G. Gao, H. Li, R. Li, *Nano Energy* **2021**, *90*, 106614.  
[S3] J. Wu, Z. Wu, X. Lu, S. Han, B-R. Yang, X. Gui, K. Tao, J. Miao, C. Liu, *ACS Appl. Mater. Interfaces* **2019**, *11*, 9405–9414.  
[S4] Q. Yu, Z. Qin, F. Ji, S. Chen, S. Luo, M. Yao, X. Wu, W. Liu, X. Sun, H. Zhang, Y. Zhao, F. Yao, J. Li, *Chem. Eng. J.* **2021**, *404*, 126559.  
[S5] Z. Xie, H. Li, H-Y. Mi, P-Y. Feng, Y. Liu, X. Jing, *J. Mater. Chem. C* **2021**, *9*, 10127–10137.  
[S6] J. Chen, Q. Yu, D. Shi, Z. Yang, K. Dong, D. Kaneko, W. Dong, M. Chen, *ACS Appl. Energy Mater.* **2021**, *4*, 9353–9361.  
[S7] N. Lu, R. Na, L. Li, C. Zhang, Z. Chen, S. Zhang, J. Luan, G. Wang, *ACS Appl. Energy Mater.* **2020**, *3*, 1944–1951.  
[S8] L. Fang, J. Zhang, W. Wang, Y. Zhang, F. Chen, J. Zhou, F. Chen, R. Li, X. Zhou, Z. Xie, *ACS Appl. Mater. Interfaces* **2020**, *12*, 56393–56402.  
[S9] Z. Qin, X. Sun, H. Zhang, Q. Yu, X. Wang, S. He, F. Yao, J. Li, *ACS Appl. Mater. Interfaces* **2020**, *8*, 4447–4456.  
[S10] W. Peng, L. Han, Y. Gao, Z. Gong, T. Lu, X. Xu, M. Xu, Y. Yamauchi, L. Pan, *J. Colloid Interface Sci.* **2022**, *608*, 396–404.  
[S11] C. Qin, A. Lu, *Carbohydr. Polym.* **2021**, *274*, 118667.  
[S12] X. Qian, A. Lu, *ACS Appl. Polym. Mater.* **2021**, *3*, 3747–3754.

- [S13] L-B. Huang, X. Dai, Z. Sun, M-C. Wong, S-Y. Pang, J. Han, Q. Zheng, C-H. Zhao, J. Kong, J. Hao, *Nano Energy* **2021**, 82, 105724.
- [S14] W. Xu, L-B- Huang, M-C. Wong, L. Chen, G. Bai, J. Hao, *Adv. Energy Mater.* **2017**, 7, 1601529.
- [S15] X. Pu, M. Liu, X. Chen, J. Sun, C. Du, Y. Zhang, J. Zhai, W. Hu, Z. L. Wang, *Sci. Adv.* **2017**, 3, e1700015.
- [S16] T. Liu, M. Liu, S. Dou, J. Sun, Z. Cong, C. Jiang, C. Du, X. Pu, W. Hu, Z. L. Wang, *ACS Nano* **2018**, 12, 2818–2826.
- [S17] Q. Guan, G. Lin, Y. Gong, J. Wang, W. Tan, D. Bao, Y. Liu, Z. You, X. Sun, Z. Wen, Y. Pan, *J. Mater. Chem. A* **2019**, 7, 13948–13955.
- [S18] J-N. Kim, J- Lee, H- Lee, I-K. Oh, *Nano Energy* **2021**, 82, 105705.
- [S19] F. Sheng, J. Yi, S. Shen, R. Cheng, C. Ning, L. Ma. X. Peng, W. Deng, K. Dong, Z. L. Wang, *ACS Appl. Mater. Interfaces* **2021**, 13, 44868–44877.
- [S20] X. Luo, L. Zhu, Y-C. Wang, J. Li, J. Nie, Z. L. Wang, *Adv. Funct. Mater.* **2021**, 31, 2104928.
- [S21] D. Yang, Y. Ni, H. Su, Y. Shi, Q. Liu, X. Chen, D. He, *Nano Energy* **2020**, 79, 105394.
- [S22] L. Wang, Y. Wang, H. Wang, G. Xu, A. Döring, W. A. Daoud, J. Xu, A. L. Rogach, Y. Xi, Y. Zi, *ACS Nano* **2020**, 14, 10359–10369.
- [S23] X. Liu, K. Cheng, P. Cui, H. Qi, H. Qin, G. Gu, W. Shang, S. Wang, G. Cheng, Z. Du, *Nano Energy* **2019**, 66, 104188.
- [S24] L. Zheng, Z-H. Lin, G. Cheng, W. Wu, X. Wen, S. Lee, Z. L. Wang, *Nano Energy* **2014**, 9, 291–300.
- [S25] Y. Yang, H. Zhang, Y. Liu, Z-H. Lin, S. Lee, Z. Lin, C. P. Wong, Z. L. Wang, *ACS Nano* **2013**, 7, 2808–2813.
- [S26] B. Dudem, Y. H. Ko, J. W. Leem, J. H. Lim, J. S. Yu, *ACS Appl. Mater. Interfaces* **2016**, 8, 30165–30175.
- [S27] X. Liu, P. Cui, J. Wang, W. Shang, S. Zhang, J. Guo, G. Gu, B. Zhang, G. Cheng, Z. Du, *Nanotechnology* **2021**, 32, 075401.
- [S28] G-H. Kim, L. Shao, K. Zhang, K. P. Pipe, *Nat. Mater.* **2013**, 12, 719–723.
- [S29] Z. U. Khan, O. Bubnova, M. J. Jafari, R. Brooke, X. Liu, R. Gabrielsson, T. Ederth, D. R. Evans, J. W. Andresen, M. Fahlman, X. Crispin, *J. Mater. Chem. C* **2015**, 3, 10616–10623.
- [S30] P. Yang, K. Liu, Q. Chen, X. Mo, Y. Zhou, S. Li, G. Feng, J. Zhou, *Angew. Chem. Int. Ed.* **2016**, 55, 12050–12053.
- [S31] J. Wu, J. J. Black, L. Aldous, *Electrochim. Acta* **2017**, 225, 482–492.
- [S32] Q. Wang, J. Li, J. Li, *Phys. Chem. Chem. Phys.* **2018**, 20, 1460–1475.
- [S33] Y. Liu, Q. Dai, Y. Zhou, B. Li, X. Mao, C. Gao, Y. Gao, C. Pan, Q. Jiang, Y. Wu, Y. Xie, L. Wang, *ACS Mater. Interfaces* **2019**, 11, 29320–29329.
- [S34] M. Bharti, A. Singj, A. K. Debnath, A. K. Chauhan, K. P. Muthe, S. K. Gupta, K. Marumoto, T. Mori, D. K. Aswal, *Mater. Today Phys.* **2021**, 16, 100307.